NANO MICRO small

Supporting Information

for *Small,* DOI: 10.1002/smll.202300148

High-Energy Aqueous Magnesium Ion Batteries with Capacity-Compensation Evolved from Dynamic Copper Ion Redox

*Shuxin Zhang, Yaowei Wang, Yukun Sun, Yaru Wang, Yang Yang, Peng Zhang, Xuecheng Lv, Jiulin Wang, Hong Zhu, and Yanna NuLi**

High-energy aqueous magnesium ion batteries with capacity-compensation evolved from dynamic copper ion redox

*Shuxin Zhang, Yaowei Wang, Yukun Sun, Yaru Wang, Yang Yang, Peng Zhang, Xuecheng Lv, Jiulin Wang, Hong Zhu, Yanna NuLi**

S. X. Zhang, Y. K. Sun, Y. R. Wang, Dr. Y. Yang, P. Zhang, Prof. J. L. Wang, and Prof. Y. N. NuLi

School of Chemistry and Chemical Engineering, Shanghai Electrochemical Energy Devices Research Center, Shanghai Jiao Tong University, Shanghai 200240, P. R. China

E-mail: nlyn@sjtu.edu.cn

Y. W. Wang, Prof. H. Zhu

University of Michigan-Shanghai Jiao Tong University Joint Institute, Shanghai Jiao Tong University, Shanghai 200240, P. R. China

X. C. Lv

School of Energy and Power Engineering, Dalian University of Technology, Dalian, 116024, P.R. China

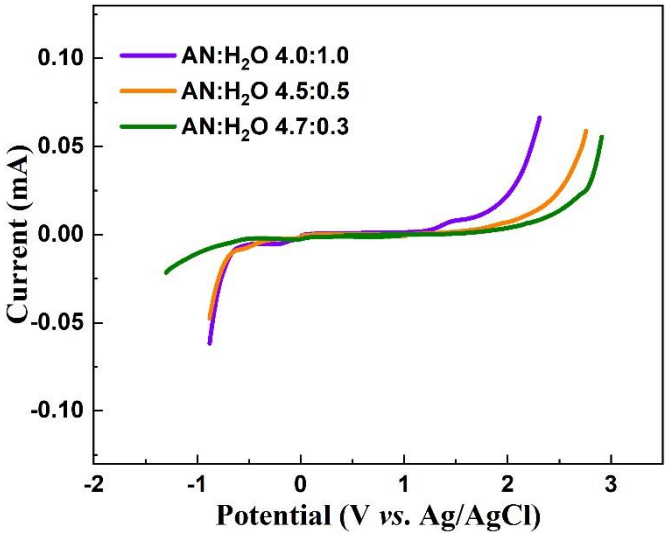

Figure S1. LSV curves showing the electrochemical windows of 1 mol L^{-1} $Mg(TFSI)_2$ in AN/H_2O hybrid electrolytes with different volume ratios of AN to H_2O.

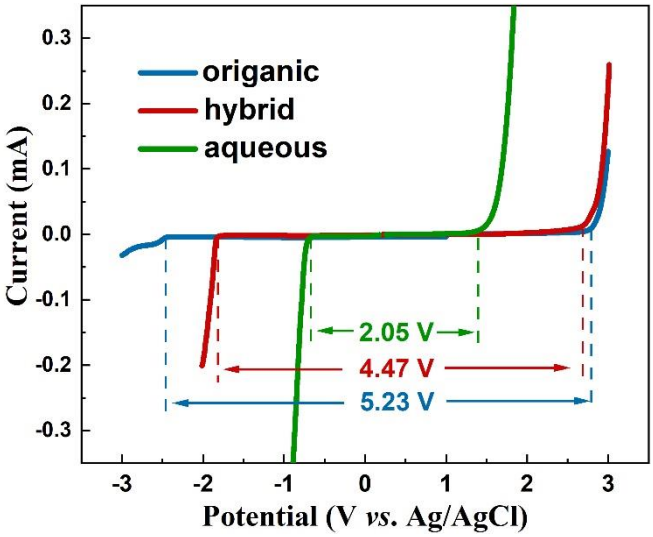

Figure S2. LSV curves showing the electrochemical windows of 1 mol L^{-1} $Mg(TFSI)_2$ in AN, H_2O and AN/H_2O (4.9:0.1) hybrid electrolytes.

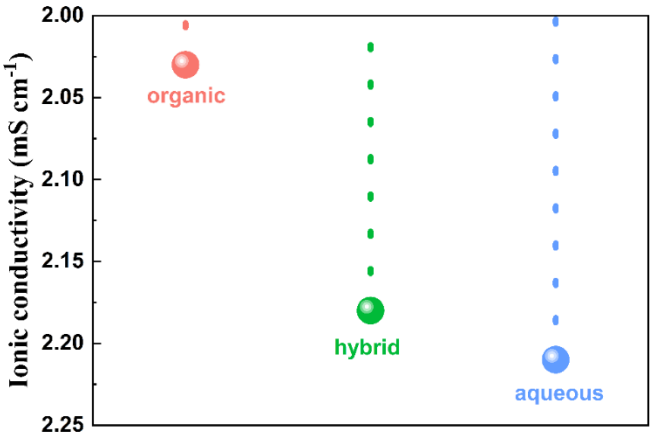

Figure S3. Ionic conductivity of 1mol L^{-1} $Mg(TFSI)_2$ in hybrid AN/H_2O, origanic and aqueous electrolytes.

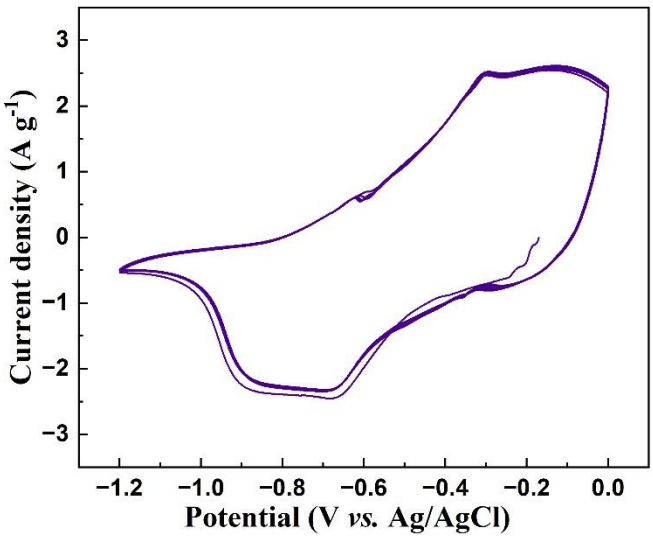

Figure S4. CV curves of PTCDI electrodes at 5 mV s^{-1} in a three-electrode system.

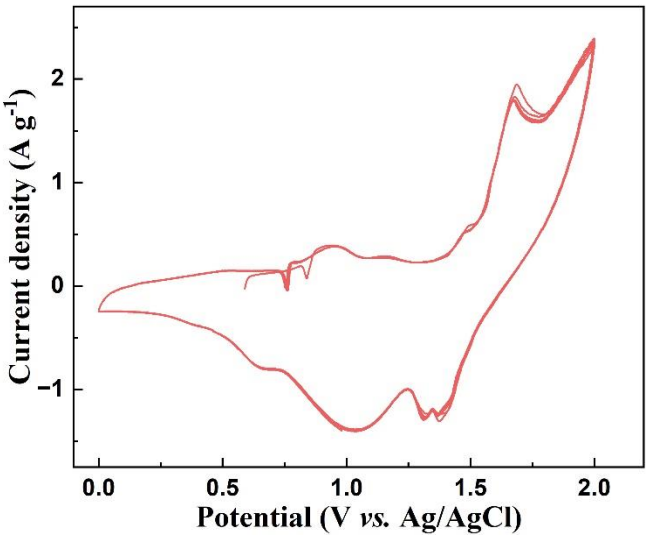

Figure S5. CV curves of EG electrodes at 5 mV s^{-1} in a three-electrode system.

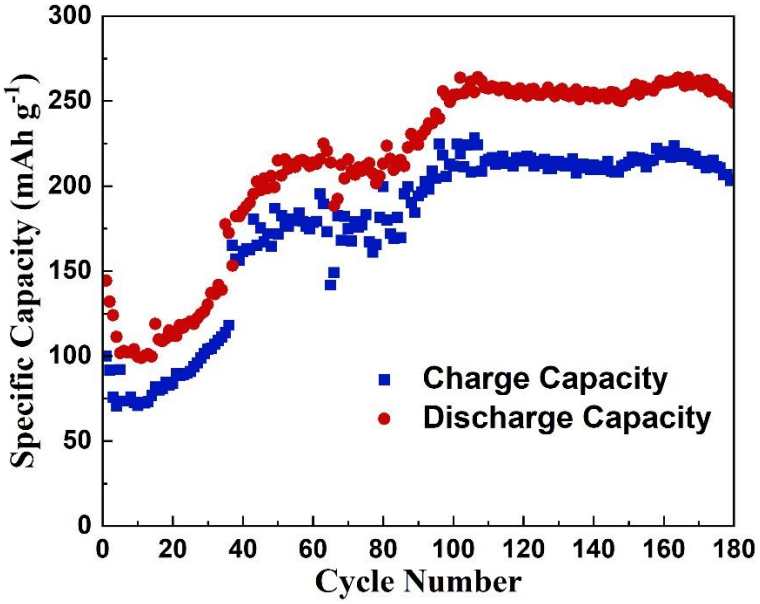

Figure S6. Cycling performance of PTCDI anode with copper foam interlayer at 5 A g^{-1} using a three electrode cell with PTCDI as the working electrode, platinum as the counter electrode and standard Ag/AgCl electrode as the reference electrode.

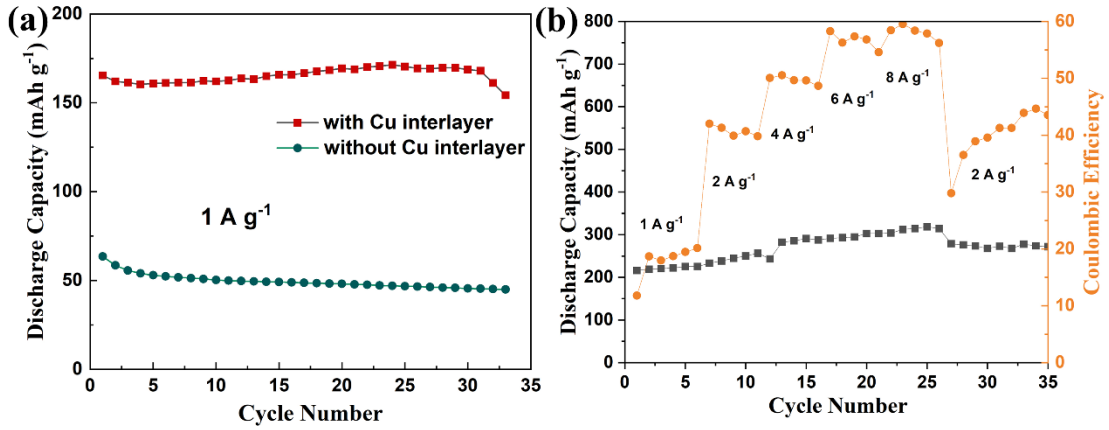

Figure S7 (a) Cycling performance of the full cells with and without Cu foam interlayer at a current density of 1 A g^{-1}; (b) Rate capability of full cell with Cu foam interlayer from the current density of 1 A g^{-1} to 8 A g^{-1}.

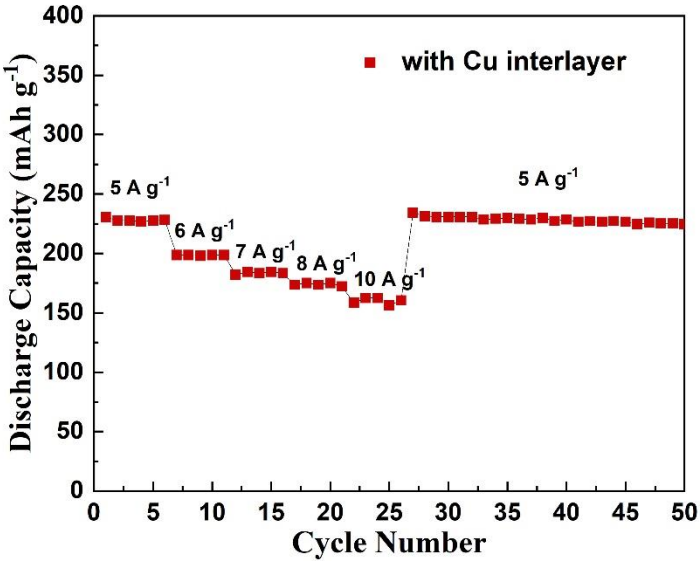

Figure S8. Rate capability of full cells with Cu foam interlayer after fully activation from the current density of 5 A g^{-1} to 10 A g^{-1}.

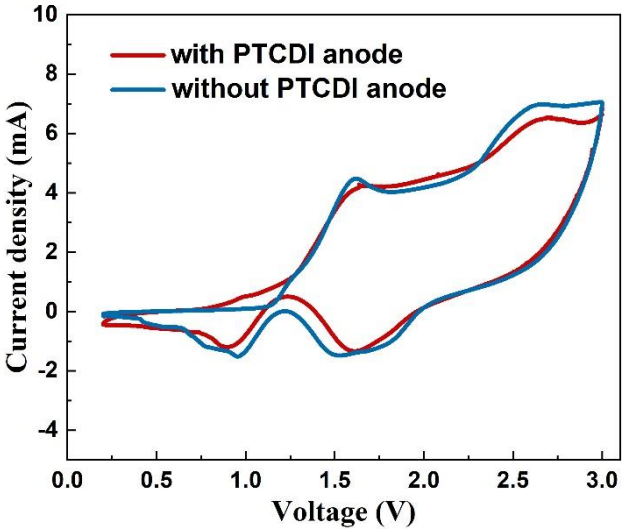

Figure S9. CV curves of full cells with and without PTCDI anode in $Cu(TFSI)_2$ electrolyte at 5 mV s^{-1}.

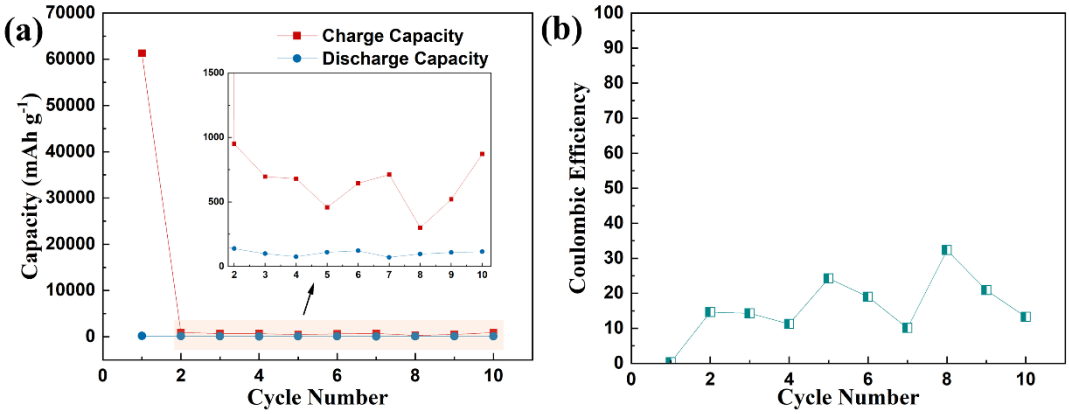

Figure S10. The cycling performance (a) and Coulombic efficiency (b) for the EG||PTCDI cell containing $Cu(TFSI)_2$ electrolyte.

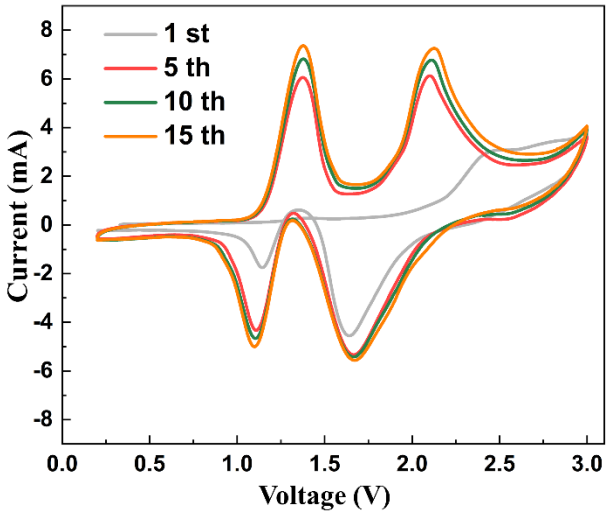

Figure S11. CV curves for different cycles of the EG||PTCDI full cell with $Mg(TFSI)_2$ electrolyte and Cu foam interlayer at a scan rate of 5 mV s^{-1}.

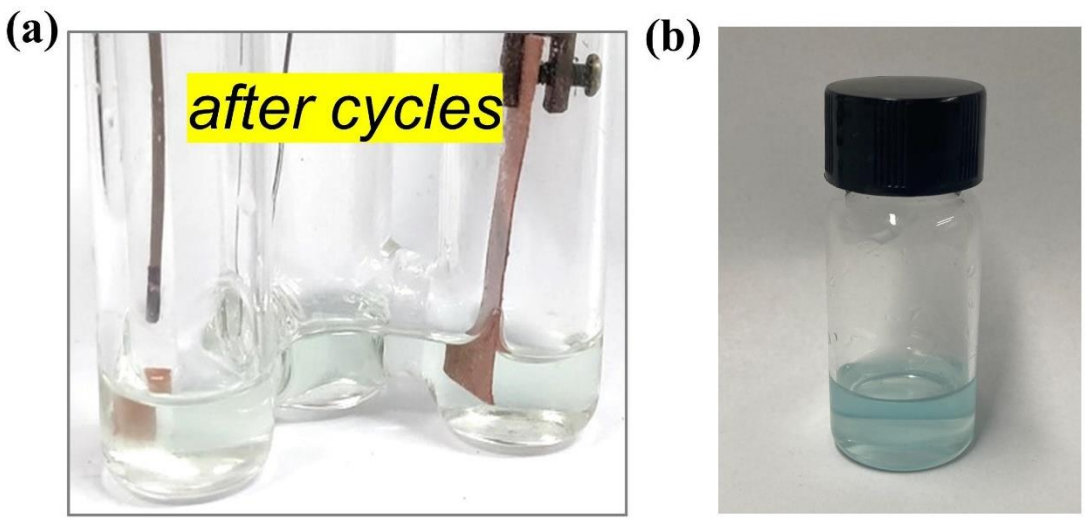

Figure S12. (a) Optical photo of a three-electrode cell system (working electrode: Cu foam; counter electrode: platinum; reference electrode: standard Ag/AgCl electrode) with $Mg(TFSI)_2$ electrolyte after three CV cycles at 5 mV s^{-1}; (b) Optical photo of 0.04 mol L^{-1} $Cu(TFSI)_2$ electrolyte.

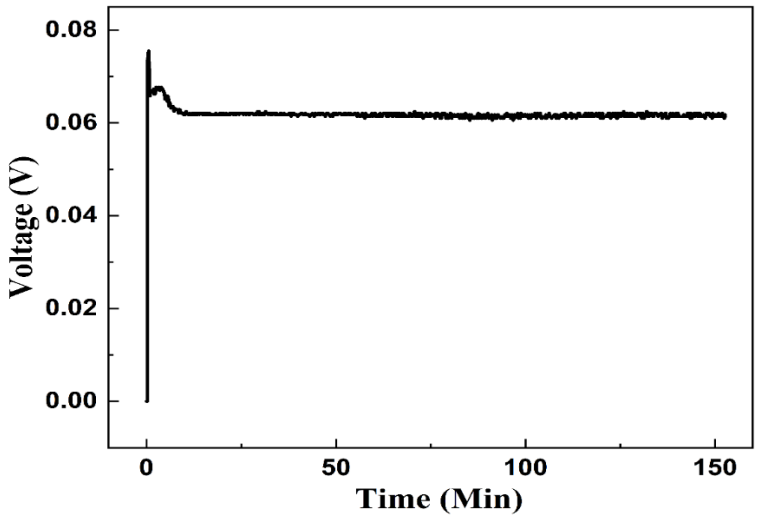

Figure S13. The voltage variation of the full cell without PTCDI active material during charging process.

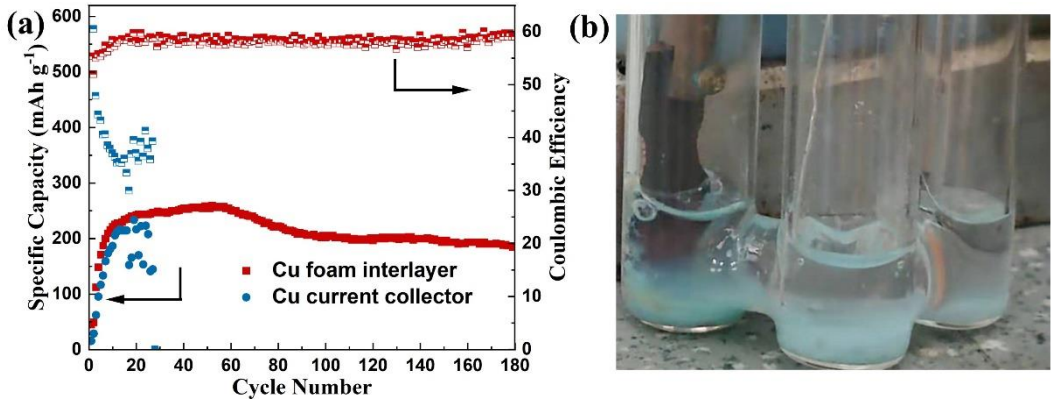

Figure S14. (a) Cycling performance of the EG||PTCDI full cells with Cu foam interlayer and carbon paper anode current collector, Cu foil directly as the anode current collector at a current density of 5 A g^{-1}; (b) Optical photo of a three-electrode cell system (working electrode: PTCDI coated on copper foil; counter electrode: platinum; reference electrode: standard Ag/AgCl electrode) with $Mg(TFSI)_2$ electrolyte after CV cycles.

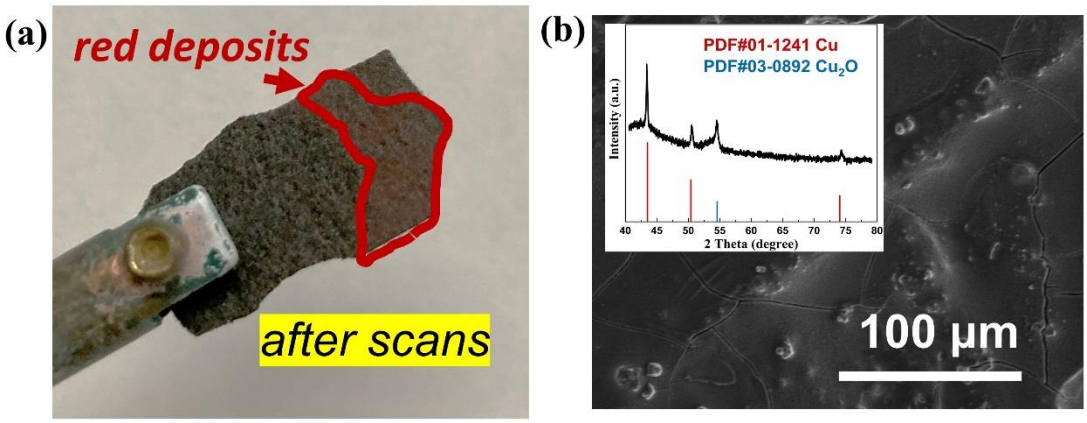

Figure S15. (a) Optical photo of carbon paper electrode after continuous negative LSV scans in a three-electrode cell system (counter electrode: platinum; reference electrode: standard Ag/AgCl electrode) at 5 mV s^{-1} with the electrolyte obtained after CV cycles of the three-electrode cell (working electrode: Cu foam; counter electrode: platinum; reference electrode: standard Ag/AgCl electrode) in $Mg(TFSI)_2$ electrolyte (Figure S12a). (b) SEM photo of carbon paper after LSV scans, inset is the XRD result.

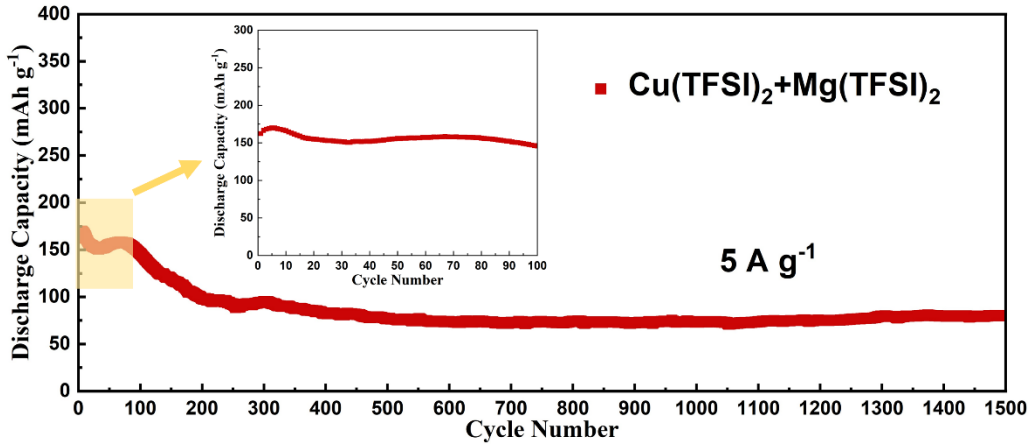

Figure S16. Cycling performance of the EG||PTCDI full cell with $Cu(TFSI)_2$+$Mg(TFSI)_2$ electrolyte at a current density of 5 A g^{-1}.

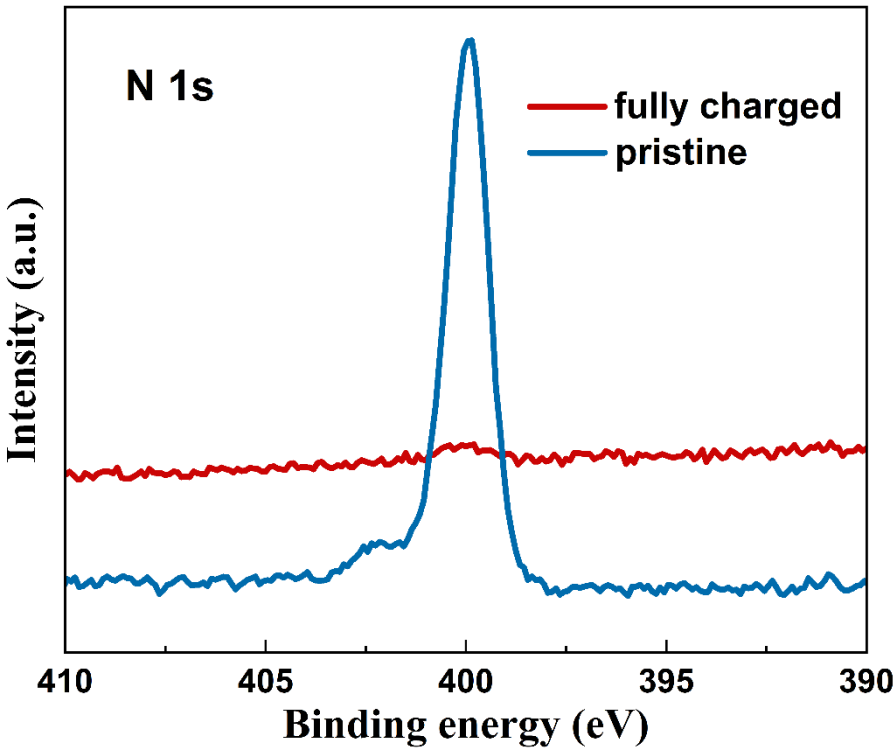

Figure S17. N 1s XPS analysis of pristine PTCDI and PTCDI anode from fully charged EG||PTCDI full cell.

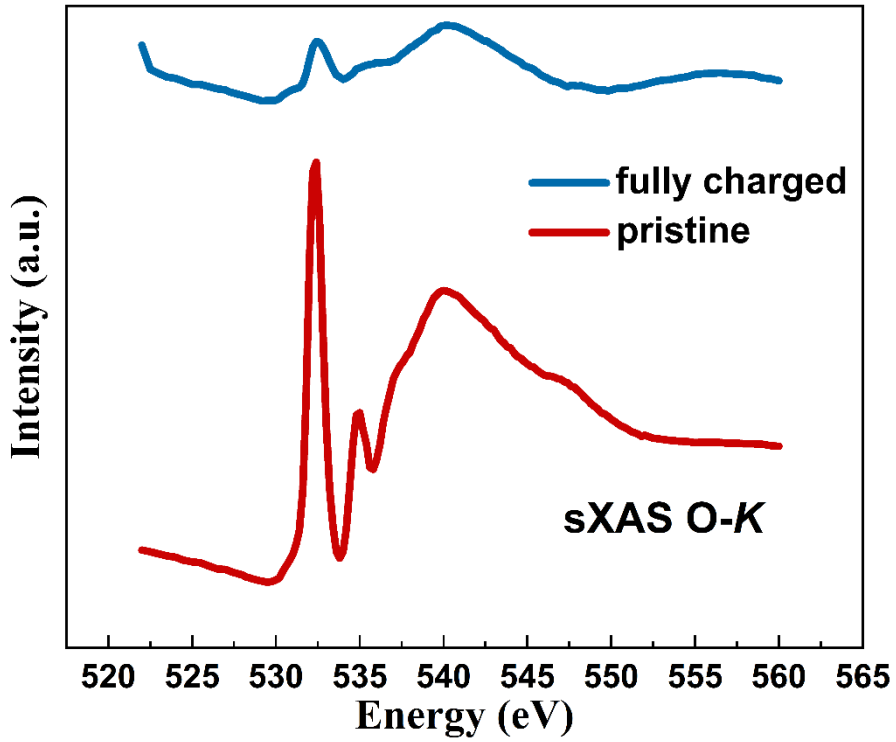

Figure S18. sXAS spectra at O *K*-edge of pristine PTCDI and PTCDI anode from fully charged EG||PTCDI full cell.

Table S1. The optimized four PTCDI-Cu structures.

Structure number	The energy after optimization ($E_{PTCDI+nCu}$)	The energy of PTCDI (E_{PTCDI})	The number of Cu (n)	The energy of single Cu (E_{Cu})	The energy of total Cu (Ne_{Cu})	Formation energy (E_f)
1	-617.20622	-603.77514	4	-4.0992	-16.3968	2.96572
2	-615.46452	-603.77514	4	-4.0992	-16.3968	4.70742
3	-610.34888	-603.77514	2	-4.0992	-8.1984	1.62466
4	-610.08014	-603.77514	2	-4.0992	-8.1984	1.89340